Applied Catalysis A: General 468 (2013) 276–287

Contents lists available at ScienceDirect

Applied Catalysis A: General

journal homepage: www.elsevier.com/locate/apcata

Sequential desilication–isomorphous substitution route to prepare mesostructured silica nanoparticles loaded with ZnO and their photocatalytic activity

N.W.C. Jusoh[a], A.A. Jalil[a,*], S. Triwahyono[b], H.D. Setiabudi[a], N. Sapawe[a], M.A.H. Satar[a], A.H. Karim[b], N.H.N. Kamarudin[a], R. Jusoh[a], N.F. Jaafar[b], N. Salamun[b], J. Efendi[b]

[a] Institute of Hydrogen Economy, Department of Chemical Engineering, Faculty of, Chemical Engineering, Universiti Teknologi Malaysia, UTM, Johor Bahru, Johor 81310, Malaysia
[b] Ibnu Sina Institute for Fundamental Science Studies, Faculty of Science, Universiti Teknologi Malaysia, UTM, Johor Bahru, Johor 81310, Malaysia

ARTICLE INFO

Article history:
Received 17 May 2013
Received in revised form 30 August 2013
Accepted 4 September 2013

Keywords:
ZnO/MSN
Mesostructured silica nanoparticles
Desilication
Isomorphous substitution
Photodecolorization

ABSTRACT

A simple electrochemical method followed by impregnation was employed to prepare a coral-like zinc oxide catalyst loaded on mesostructured silica nanoparticles (ZnO/MSN). The introduction of zinc species onto a silica framework was found to form an interaction between the host and support material. XRD analysis suggested the presence of zinc on the internal pore walls of MSN. FE-SEM and TEM analyses displayed nanorods, nanoparticles and coral-like shapes of ZnO, MSN and ZnO/MSN, respectively. ^{29}Si NMR and FTIR results showed that desilication occurred in the silica framework of the MSN accompanied by isomorphous substitution of Zn^{2+} cations to form an active species Zn–O–Si bond. The photocatalytic activity of the ZnO/MSN was tested by decolorizing methyl orange (MO). It was found that increasing the ZnO loading led to a higher recombination rate of photoinduced electron–hole pairs, which resulted in decreased photocatalytic activity. The highest decolorization rate was obtained using 1 g L^{-1} of 5 wt% ZnO/MSN with an optimum dosage of 3.06×10^{-2} mM MO after 8 h contact time at pH 2 under UV irradiation. A kinetic study demonstrated that the photocatalytic reaction followed the pseudo first-order model. The photocatalyst was still stable after five cycling runs with a small amount of Zn was leached (<3.0%).

1. Introduction

Dyes widely used in the textile, paper, cosmetics and plastics industries have led to severe environmental contamination due to their emission of toxic and colored wastewater into water bodies [1]. This phenomenon seriously affects the nature of water, inhibits sunlight penetration and reduces photosynthetic reactions. In addition, some dyes are either toxic or carcinogenic. Many treatment methods including biological, adsorption, coagulation and flocculation, ion exchange and membrane separation have been reported for the removal of dyes to varying degrees [2–7]. However these methods are usually non-destructive, inefficient and costly or just transfer pollutants from water to another phase.

An advanced oxidation process (AOPs) using heterogeneous semiconductor photocatalysts such as TiO_2, Fe_2O_3, ZnO, CuO, ZrO_2, CdS, and SnO_2 can be an alternative to conventional methods for the removal of dye pollutants from water [8,9]. Among them, ZnO has become very well established in photocatalytic approaches as well as in the environmental catalysis area. The photocatalytic activity of ZnO was recently recognized to be comparable with TiO_2 and has received much attention because of its unique properties and numerous advantages, such as high photosensitivity and stability in degrading various toxic substances [10]. However, even though ZnO has sufficient photocatalytic activity, photodegradation of diluted pollutants cannot proceed efficiently because of insufficient contact with the catalyst surface, which is an important factor in hindering photocatalytic activity. The mass transfer to the catalyst surface limits the photodegradation rate of diluted pollutants [11]. Thus, a suitable method to improve the contact between pollutant molecules and a catalyst should be found in order to enhance the adsorption of pollutant molecules. One method is incorporation of ZnO into a mesoporous material support, which has been discussed by several research groups in recent years [12–14]. A review of recent studies revealed some important supports for ZnO, including HZSM-5, SiO_2, MCM-41 and MCM-22 [15–17].

Recently, we reported a new electrochemical method for preparation of metal oxide nanoparticles including ZrO_2, α-Fe_2O_3, CuO and ZnO [18–21]. Further loading of these nanometal oxides onto

* Corresponding author. Tel.: +60 7 5535581; fax: +60 7 5536165.
E-mail address: aishah@cheme.utm.my (A.A. Jalil).

0926-860X/$ – see front matter © 2013 Elsevier B.V. All rights reserved.
http://dx.doi.org/10.1016/j.apcata.2013.09.005

zeolite supports led to enhanced catalytic activity, which was exhibited by efficient photodecolorization of various dyes as well as isomerization of *n*-alkane [18–20,22–24]. It was found that in most cases, dealumination accompanied by isomorphous substitution readily occurred in the aluminosilicate framework of the zeolites during preparation of these catalysts, which then improved their properties toward the subsequent reactions. Thus, we anticipated a similar perturbation occurs in the framework of mesoporous silica when using a similar simple electrolysis system. This would be of interest because silica is recognized as a less active material for many heterogeneous catalytic reactions due to the absence of active sites. Immobilization of a metal onto an inexpensive silica support would improve its acidic properties and thus activate the catalyst [25]. To our knowledge, reports on desilication accompanied by isomorphous substitution of foreign ions such as Zn for Si in a silica framework are still scanty. In addition, most ZnO studied were nanoparticles, but little information has been reported for alternate shapes of supported ZnO.

Therefore, in this study we report for the first time the preparation of ZnO supported on mesostructured silica nanoparticles (MSN) and its photocatalytic performance toward decolorization of methyl orange (MO). In fact, the MSN used has a large surface area with a uniform and tunable pore size, which offers considerable potential as an excellent solid support for immobilization of heterogeneous catalysts [26]. The tortuous and winding shape of the coral-like ZnO/MSN is expected to afford a larger surface area for favorable results. The prepared catalyst was characterized by X-ray diffraction (XRD), field emission scanning electron microscopy coupled with energy dispersive X-ray (FE-SEM/EDX), transmission electron microscopy (TEM), ^{29}Si magic angle spinning nuclear magnetic resonance (MAS-NMR), Fourier transform infrared (FTIR), adsorbed pyridine and carbon monoxide FTIR, photoluminescence (PL), and Brunnauer–Emmett–Teller (BET) surface area analysis. A new structural model for ZnO/MSN was proposed on the basis of the literature, characterization and photodecolorization results. The decolorization of MO was optimized under various parameters such as the effect of pH, catalyst dosage, and ZnO loading. The kinetic behavior of the catalyst was also studied to determine the rate constant.

2. Experimental

2.1. Materials

Cetyltrimethylammonium bromide (CTAB), ethylene glycol (EG), tetraethyl orthosilicate (TEOS), methyl orange (MO), 3-aminopropyl triethoxysilane (APTES), sodium hydroxide (NaOH), and hydrochloric acid (HCl), were purchased from MERCK Sdn. Bhd., Malaysia. Ammonium hydroxide solution (NH_4OH) was obtained from QRec, Malaysia. The platinum and zinc plates of more than 99.99% purity were obtained from Nilaco Metal, Japan. Tetraethylammonium perchlorate (TEAP), which was used as a supporting electrolyte in electrolysis, was prepared in accordance with the procedure reported in the literature [27]. Deionized water was used for the preparation of the pH solution and adjustments to the pH were performed using a 0.1 M HCl and NaOH solution.

2.2. Catalyst preparation

The mesostructured silica nanoparticles (MSN) were prepared by a co-condensation and sol–gel method as reported in previous literature [26]. The CTAB surfactant, EG, and NH_4OH solution were dissolved in 700 mL of water with the mole composition of CTAB:EG:NH_4OH:H_2O were 0.0032:0.2:0.2:0.1, respectively. After vigorous stirring for about 30 min with heating, 1.2 mmol TEOS and 1 mmol APTES were added to the clear mixture to give a white suspension solution. This solution was then stirred for another 2 h, and the samples were collected by centrifugation. The synthesized MSN were dried at 333 K and calcined at 823 K for 3 h to remove the surfactant.

The ZnO nanorods were prepared according to previous reported protocol with some modification [28,29]. An open system electrolysis cell was fitted with a magnetic stirrer and a platinum plate cathode ($2 \times 2\,cm^2$) facing a zinc plate anode ($2 \times 2\,cm^2$). A 10 mL distilled water and 4 mL NH_4OH were added into a 0.1 M CTAB and 0.1 M TEAP, which act as a capping agent and supporting electrolyte, respectively. The electrolysis was conducted at a constant current of 120 mA cm^{-2} and 0 °C under air atmosphere. After electrolysis, the obtained mixture was impregnated and dried at 383 K for 12 h before being calcined at 823 K for 3 h to yield grayish ZnO nanorods.

The ZnO/MSN catalyst was prepared via the same procedure as ZnO nanorods, except the MSN was added to the mixture after electrolysis. The mixture was then impregnated, dried and calcined as above to give a white powder catalyst which is ready for a characterization. The required weight of the ZnO supported on the MSN was calculated based on duration time of the electrolysis according to the Faraday's law of electrolysis as follows:

$$t = \left(\frac{F}{I}\right)(z \times n) \quad (1)$$

where t is a total time for the constant current applied (s); F is a Faraday constant, 96,486 C mol^{-1}; I is an electric current applied; z is a valency number of ions of substances (electrons transferred per ion); and n is an amount of substance (number of moles, liberated $n = m/M$).

2.3. Characterization

The crystalline structures of the catalysts were studied by XRD recorded on a D8 ADVANCE Bruker X-ray diffractometer using Cu $K\alpha$ radiation at a 2θ angle ranging from 2° to 90°. The phases were identified with the aid of the Joint Committee on Powder Diffraction Standards (JCPDS) files.

The morphological properties of ZnO, MSN and ZnO/MSN catalysts as well as the dispersion of ZnO onto MSN surface were examined by field emission scanning electron microscopy (FESEM) (JSM-6300F FESEM) with energy dispersion X-ray (EDX) and transmission electron microscopy (TEM).

The textural properties (i.e., specific surface area, pore volume, and pore diameter) were determined from nitrogen physisorption at 77 K using a Quantachrome Autosorb-1 analyzer. Prior to measurements, the samples were evacuated for 24 h at 573 K. Specific surface area (S_{BET}) values were calculated from the BET isotherm plots, while the total pore volume and pore size distributions were calculated using the Barrett, Joyner, and Halenda (BJH) method from the desorption isotherm.

Nuclear magnetic resonance measurements were carried out using ^{29}Si magic angle spinning nuclear magnetic resonance (MAS-NMR) Spectroscopy, which was performed at room temperature on a Bruker Solid NMR (JEOL 400 MHz) spectrometer using tetramethylsilane (TMS) as an external reference. The spectra were recorded using 4 μs radio frequency pulses, a recycle delay of 60 s and spinning rate of 7 kHz using a 4 mm zirconia sample rotor.

FT-IR (Perkin Elmer Spectrum GX FTIR Spectrometer) was performed using the KBr method with a scan range of 400–4000 cm^{-1}. IR spectroscopy of adsorbed pyridine was used as a tool to evaluate the Brönsted and Lewis acid sites. In addition, carbon monoxide was used to evaluate the active sites on the ZnO/MSN catalyst. Before the analysis, catalyst was activated according to the method described in the literature [24]. In brief, a self supported wafer placed in an

in situ IR cell with CaF_2 windows was heated at 673 K for 1 h. The adsorption of pyridine (2 Torr) was conducted at 423 K for 15 min, followed by outgassing at 573 K for 30 min. For carbon monoxide (10 Torr), the adsorption was conducted at room temperature for 30 min followed by decreasing the temperature to 123 K. All spectra were recorded at room temperature. In order to compare the surface coverage of the adsorbed species between different wafer thicknesses, all spectra were normalized using the overtone and combination vibrations between 2100 and 1550 cm^{-1} after activation.

The photoluminescence (PL) (JASCO Spectrofluorometer) (FP-8500) with 150 W Xe lamp as excitation source were employed to study the electronic structure, optical and photochemical properties of semiconductor materials, by which information such as surface oxygen vacancies and defects can be obtained.

The powder addition method was performed to measure a point zero charge (pH_{pzc}) of the catalyst as described in the literature [30]. A set of distilled water were prepared (40 mL) and the pH were adjusted to 2, 5, 7, 9 and 11 using NaOH and HCl. The initial pH (pH_i) was recorded and an amount of catalyst was added to each solution. The solution was stirred and the final pH (pH_f) was measured after 48 h. The value of final minus initial pH (ΔpH) is plotted vs. pH_i. The PZC occurs at the point where $pH_f - pH_i = 0$.

2.4. Photocatalytic testing

The photoactivities of the ZnO and ZnO/MSN were evaluated for the decolorization of MO dye. The photocatalytic experiments were performed in a batch reactor fixed with UV lamp (4×9 W; 365 nm emission) and a cooling system. 1 g L^{-1} of catalyst was added to the MO solution with a desired concentration (3.06×10^{-2} mM) and stirred for 1 h in a dark to achieve adsorption–desorption equilibrium. The initial pH of the solution was 2 and the reaction was carried out at 30 °C. Then, the reaction was carried out for another 8 h under light irradiation under continuous stirring. The concentration of MO dye in the solution prior to irradiation was used as the initial value for the MO decolorization measurements. The samples were then collected at regular interval of 1 h and centrifuged in a Hettich Zentrifugen Micro 120 at 75,000 rpm for 10 min before being analyzed by UV–Vis spectrophotometer (Thermo Scientific Genesys10uv Scanning) for the residual concentration of MO. The MO decolorization was measured at the maximum adsorption peak at 506 nm.

The elemental analyses of zinc in solution were determined by microwave plasma-atomic emission spectrometer (MP-AES) using 4100 MP-AES Agilent Technologies model 98000A.

3. Result and discussion

3.1. Characterization of catalysts

3.1.1. Phase, crystallinity and structural studies

Fig. 1A illustrates a wide-angle XRD pattern of the synthesized ZnO. A series of peaks were observed at 31.8° (1 0 0), 34.5° (0 0 2), 36.3° (1 0 1), 47.6° (1 0 2), 56.7° (1 1 0), 62.9° (1 0 3), 66.4° (2 0 0), 68.0° (1 1 2), 69.1° (2 0 1), 72.3° (0 0 4), 76.8° (2 0 2), 81.1° (1 0 4) and 89.5° (2 0 3), which can be indexed as a wurtzite ZnO structure as compared to the data from JCPDS No. 36-1451 demonstrated by the red line [31]. No other peak was found, indicating the purity of the ZnO. In fact, the structure of ZnO could be determined by the change in relative intensity of the (1 0 0) and (0 0 2) peaks [32]. The small (1 0 0)/(0 0 2) ratio indicates the formation of rods oriented along the *c* axis. Conversely, a very large (1 0 0)/(0 0 2) ratio is indicative of shortening along the *c* axis (plate-like particles) [33]. Based on the ratio shown in Fig. 1A, the structure of the electrosynthesized

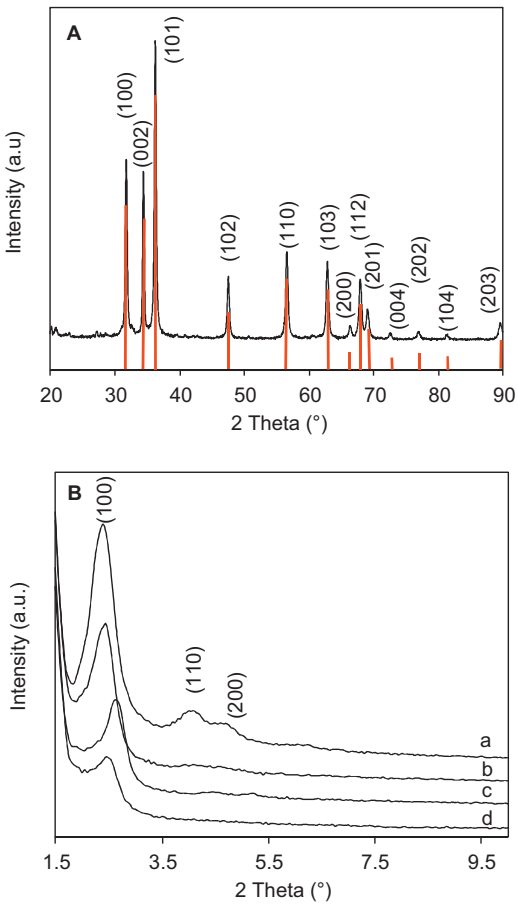

Fig. 1. (A) Wide-angle XRD patterns of synthesized ZnO and (B) small-angle XRD patterns of (a) MSN and (b) 1 wt% ZnO/MSN, (c) 5 wt% ZnO/MSN, (d) 10 wt% ZnO/MSN samples.

ZnO was presumably rod-like in shape ($Ratio_{(1\,0\,0)/(0\,0\,2)} = 1.10$). The value of interplanar distance (d-spacing) of the (0 0 2) lattice planes was 0.26 nm. Similar results had been reported in the literature on the subject of shape-controlled synthesis of rod ZnO [34]. The effect of introducing ZnO into the structure of mesostructured silica nanoparticles (MSN) was also studied using low-angle XRD patterns in the range of $2\theta = 1.5°–10°$ (Fig. 1B). Three main diffraction peaks were observed at $2\theta = 2.39°$, 4.05° and 4.71°, relative to the (1 0 0), (1 1 0) and (2 0 0) reflections, respectively (Fig. 1Ba), which corresponded to *p6mm* hexagonal symmetry in the mesostructured silica [35]. The relatively high intensity of the (1 0 0) peaks illustrates the MSN structure was produced with a highly ordered arrangement of channels [35]. The introduction of ZnO into MSN seems did not change the hexagonal structure of the support too much (Fig. 1Bb–d). However, the peak (1 0 0) intensity was decreased, while the other two peaks were almost eliminated by increasing the amount of ZnO, especially for 10 wt% ZnO/MSN, signifying the MSN structure was slightly disrupted by the incorporation of ZnO into the silica framework. In addition, the (1 0 0) reflection peak was also shifted to slightly higher angles, suggesting the presence of ZnO on the internal pore walls of the MSN. A similar phenomenon was reported when ZnO nanoparticles were incorporated on mesoporous MCM-41, which led to a decrease in uniformity and ordering in the mesoporous structure [36].

3.1.2. Morphological studies

The morphological properties of ZnO, MSN and the ZnO/MSN catalysts were investigated by field emission scanning electron microscopy (FESEM) while energy dispersion X-ray (EDX) was

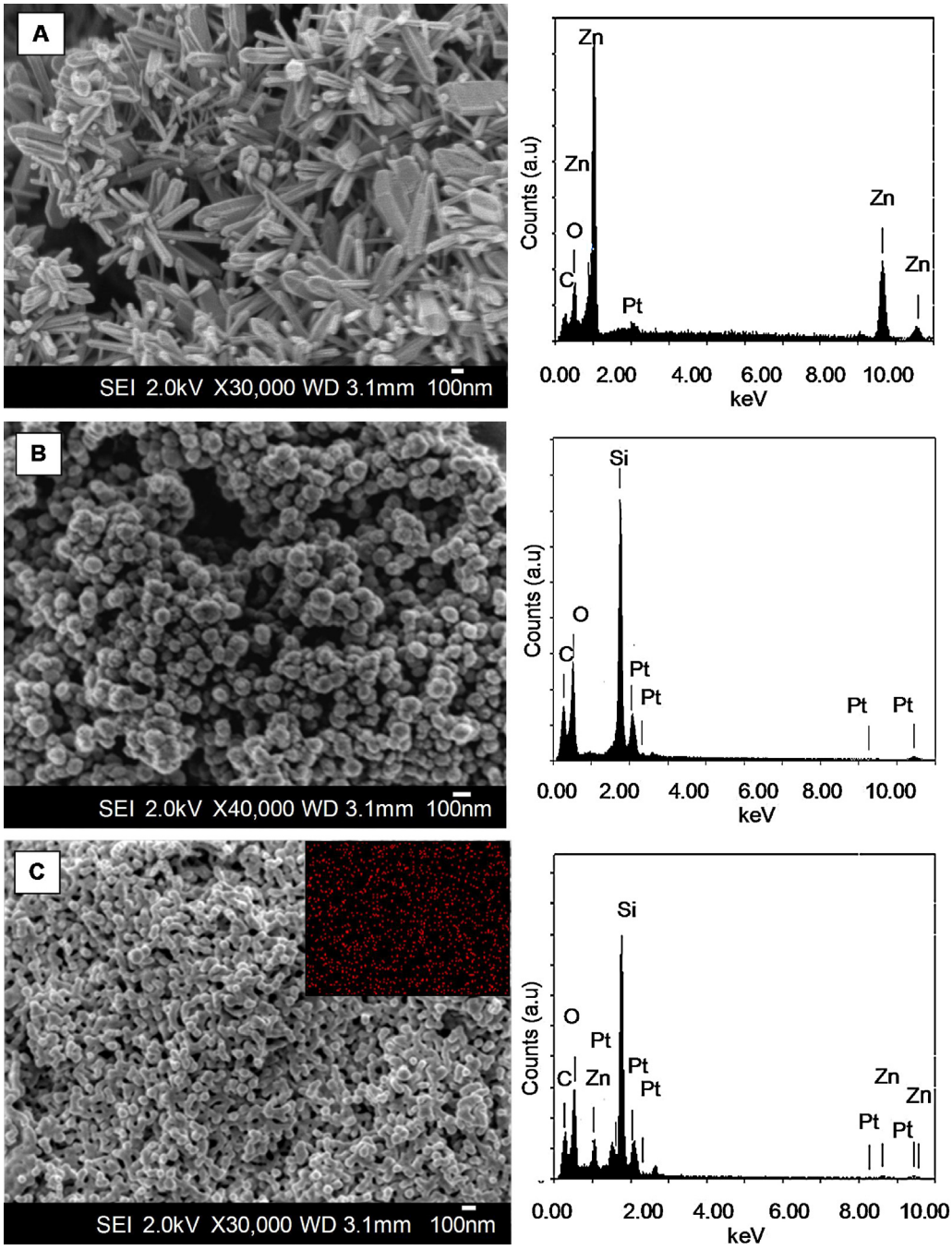

Fig. 2. FESEM–EDX images of (A) ZnO, (B) MSN and (C) 5 wt% ZnO/MSN samples.

carried out to identify the chemical composition of the catalysts (Fig. 2). It can be seen that the flower-like wurtzite shaped ZnO was successfully synthesized with multi-rods centered on one point with length and diameter of approximately 3 and 80 nm, respectively (Fig. 2A) [37]. This result was in agreement with the XRD analysis, which presupposed the rod shape of the ZnO. The EDX spectrum confirmed the presence of zinc and oxygen elements in the sample. Fig. 2B visualizes the MSN as fairly uniform spherical particles with an average diameter of 100 nm, and the EDX spectrum showed the strong signal of Si elements. Coral-shaped rods with a diameter and length around 50 and 150 nm were observed for ZnO/MSN sample as shown in Fig. 2C. The EDX spectrum of the impregnated network confirmed the presence of Zn in the MSN support. Peaks of all elements constituting the sample, including carbon from the stub and the platinum of the coating, were also recognized. In addition, the dispersion of Zn in the sample was observed by EDX mapping as shown in the inset Fig. 2C.

In order to further explore the structural features of the catalysts, the ZnO, MSN and ZnO/MSN were subjected to transmission electron microscopy (TEM); the results are shown in Fig. 3. TEM also revealed the rod-like nanostructures of flower-like ZnO with diameters around 100 nm and lengths up to several micrometers (Fig. 3A). The inset figure indicates that the interplanar spacing of the lattice planes was 0.259 nm, which matches well with the distance value of (0 0 2) lattice planes from the XRD pattern. This provided evidence for the single-crystal formation of the nanorod [38]. The TEM image in Fig. 3B clearly shows the well-ordered pores corresponded to a 2D hexagonal *p6mm* mesostructure. These

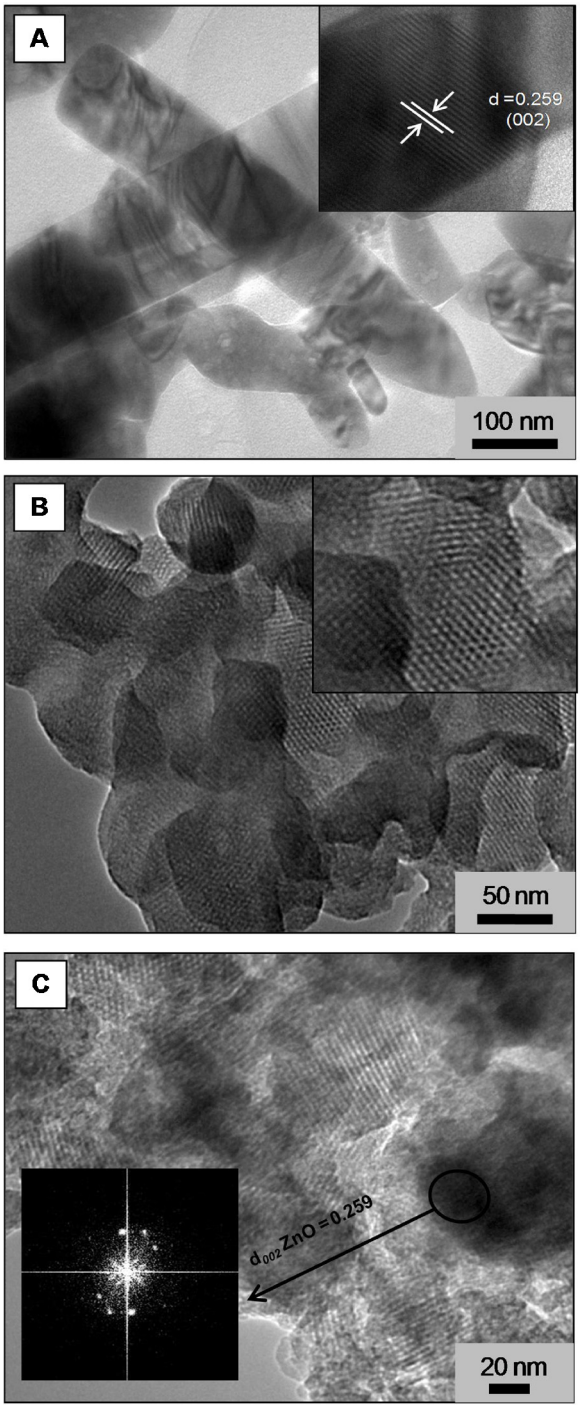

Fig. 3. TEM images of (A) ZnO, (B) MSN and (C) 5 wt% ZnO/MSN samples.

observations are in accordance with those measured in the low-angle XRD patterns. The TEM image of a 5 wt% ZnO/MSN sample in Fig. 3C also shows hexagonal pores, indicating that the ordered mesostructure has been preserved during the incorporation of ZnO. The black circular spots apparently are representative of ZnO. The rod shapes of ZnO was unable to identify, most probably it went through changes in shaped during the loading process. However, the fast Fourier transform (FFT) pattern in the inset figure confirms that the spots are due to diffraction from atoms in the corresponding planes of the wurtzite structure of ZnO. A similar image was observed during the preparation of a ZnO–SiO_2 core–shell nanorod composite [39].

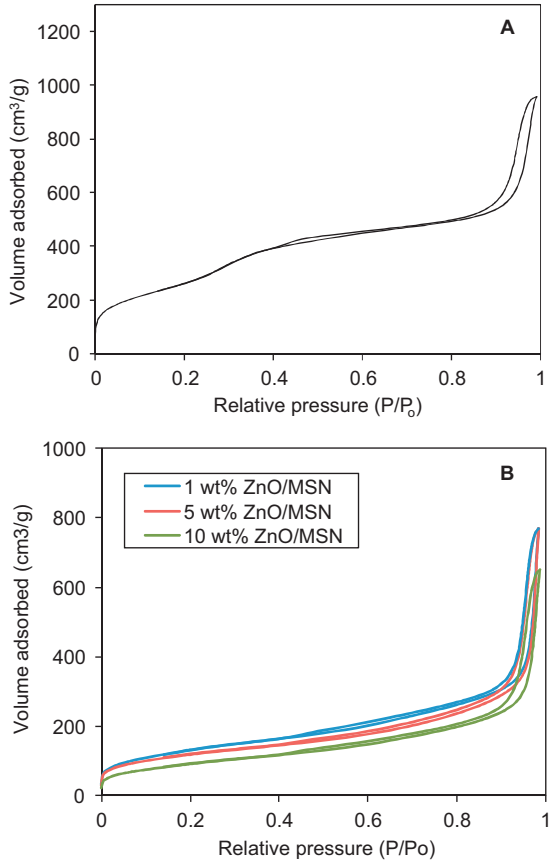

Fig. 4. N_2 adsorption–desorption isotherm plots of (A) MSN and (B) ZnO/MSN samples.

3.1.3. Study of textural properties

The adsorption–desorption isotherms of N_2 were used to study changes in the pore structure of the ZnO/MSN samples upon different ZnO loadings (Fig. 4). In Fig. 4A, a typical type IV isotherm with H1 hysteresis loop was observed for MSN [36]. The small hysteresis loops is a characteristic of uniform mesoporous materials of the M41S family with a narrow pore diameter. The inflection that occurs at $P/P_0 > 0.25$ represented spontaneous filling of the mesopores due to capillary condensation [40]. It can be observed that the characteristic pore filling step of the isotherm nearly disappears after ZnO loading (Fig. 4B), indicating that most of the channels have been packed with ZnO clusters [41]. The summary data on specific surface areas, average pore volumes and pore sizes of MSN and the ZnO/MSN catalysts are tabulated in Table 1. In all cases, it can be seen that the specific surface area and pore volume decreased after ZnO loading, suggested that a portion of the ZnO was dispersed in the pores of the MSN. This result is in agreement with the XRD, confirming the change from the well-ordered structure of MSN to reduced crystallinity upon loading of ZnO. On the contrary, the pore size was increased for all samples, suggesting the accumulation of ZnO molecules along the pore mouth that resulted in enlargement of the pore width. It could also be that the increase in pore size may be due to the larger transition metal ion size, resulting in a greater metal oxygen bond length (Zn–O) than the Si–O bond. A similar result was reported in the literature when vanadium ions were incorporated in a silica framework [42].

3.1.4. Nuclear magnetic resonance

^{29}Si Solid-state Magic Angle Spinning Nuclear Magnetic Resonance (MAS NMR) analysis of the MSN and 5 wt% ZnO/MSN catalysts were carried out to determine the ordering of the Si

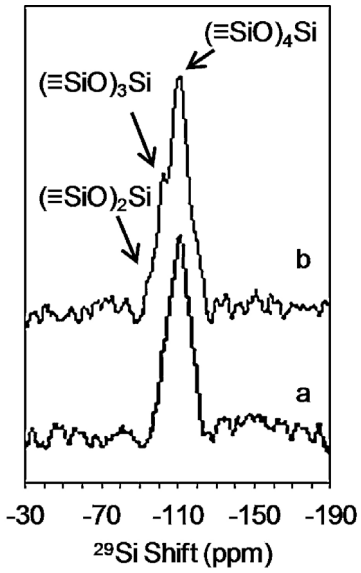

Fig. 5. ^{29}Si MAS NMR spectra of (a) MSN and (b) 5 wt% ZnO/MSN.

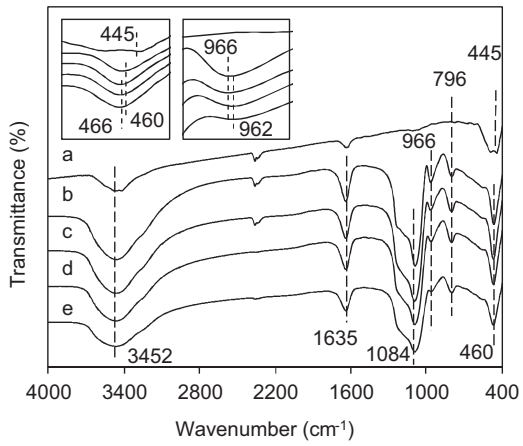

Fig. 6. FTIR spectra of (a) ZnO, (b) MSN, (c) 1 wt% ZnO/MSN, (d) 5 wt% ZnO/MSN and (e) 10 wt% ZnO/MSN.

atoms in the MSN framework; the results are illustrated in Fig. 5. With pure MSN, a dominant signal was observed at −111.4 ppm that is assigned to silicon atoms at the Q^4 site $(\equiv SiO)_4Si$ [43]. Two new shoulder peaks appeared at −98 and −92 ppm when ZnO was introduced into the MSN, indicating the formation of $(\equiv SiO)_3Si$ and $(\equiv SiO)_2Si$, respectively. Thus, it is suggested that desilication occurred in the MSN framework; this result was in agreement with the XRD results that demonstrated a decrease in intensity of the MSN peak by the introduction of ZnO. It was seen that the intensity of the peaks were not significantly affected by the desilication; this may be due to the fact that the NH_4OH solution used in preparation of the ZnO/MSN was a weak base, as compared to the strong inorganic base NaOH, which had a capacity to undergo desilication to a greater extent within short treatment times, as reported in the literature [44]. Next, the extent of the desilicated moieties was further confirmed by IR studies.

3.1.5. Vibrational spectroscopy

Fig. 6 shows the FTIR spectra of ZnO, MSN and 1–10 wt% ZnO/MSN catalysts in the region between 4000 and 400 cm^{-1}. For the ZnO sample, a broad doublet band at 445 cm^{-1} can be assigned to the ZnO stretching frequency of Zn–O bond [45]. A broad band at 3452 cm^{-1} was observed for all samples, attributable to adsorbed H_2O molecules. This band decreased in intensity with increasing amounts of ZnO loading (Fig. 6b–e), suggesting that the greater the amount of ZnO loaded onto the MSN, the fewer hydroxyl groups were adsorbed on the catalyst's surface. The band at 1635 cm^{-1} corresponds to water molecules retained by siliceous materials [26]. This band also shows a similar pattern with the band at 3452 cm^{-1}, which became smaller with increasing ZnO content and shifted slightly to a lower wavenumber, particularly with 10 wt% ZnO/MSN, signifying the possible interaction of ZnO with the silica support. A similar result was also reported in the literature, stating the appearance of a Zn–OH bond replacing the Si–OH bond in the MCM-41 structure [40]. Thus, it is suggested that the decrease in this band also demonstrates desilication as a consequence of the introduction of Zn into the silica framework. The bands at 1084, 796 and 460 cm^{-1} can be assigned to the asymmetric stretching, symmetric stretching and bending vibrations of Si–O–Si, respectively [46]. The introduction of Zn species (1–10 wt%) into the MSN also seemed to decrease the intensities of all three bands and the bands were also slightly shifted from their original positions, implying perturbation of the silica network due to the Zn–O–Si interaction. This result also can be confirmed by a Gaussian curve-fitting which plotted for the band at 460 cm^{-1} (Fig. 7). For MSN, four bands characteristic of Si–O–Si are clearly seen, but there are only three bands are present in 5 wt% ZnO/MSN. This observation supported the interaction of Zn with silica framework. Furthermore, a band at 966 cm^{-1} associated with Si–OH bending vibrations was found to decrease with increased ZnO content and be slightly shifted to 962 cm^{-1} (inset Fig. 6), which also gives evidence of Si–O–Zn bond formation [40].

For further investigation, the catalysts were evacuated at 673 K for 1 h prior to FTIR measurement to remove physisorbed water; the results are shown in Fig. 8. The narrow band at 3740 cm^{-1} is assigned to terminal silanol groups located on the external surface of the silica framework. This band partially decreased in intensity and also shifted slightly to 3737 cm^{-1} (inset figure) with the addition of Zn species onto the MSN, suggesting a perturbation of the silica framework upon interaction with the ZnO. A new broad shouldered band appeared at 3590–3480 cm^{-1}, which assigned to the presence of $Si(OH)_4$. Similar phenomena were reported in the literature on desilication of ZSM-5 and ZSM-12 zeolites [47]. These results may explain the fate of eliminated silica species in $(\equiv SiO)_4Si$ sites when they transformed to $(\equiv SiO)_3Si$ and $(\equiv SiO)_2Si$ sites, as mentioned in the ^{29}Si MAS NMR results. Baseline correction of the

Table 1
The textural properties and *d*-value of the catalysts.

Catalyst	Surface area ($m^2\ g^{-1}$)	Pore volume ($cm^3\ g^{-1}$)	Average pore size[c] (nm)	*d* value (Å)
ZnO	42	9.64×10^{-3}	33.6	2.60[a]
MSN	961	1.60	5.46	36.7[b]
1 wt% ZnO/MSN	484	1.21	10.4	36.7[b]
5 wt% ZnO/MSN	432	1.19	11.5	35.3[b]
10 wt% ZnO/MSN	345	1.04	12.5	33.3[b]

[a] *d* value at (0 0 2).
[b] *d* value at (1 0 0).
[c] Average pore size obtained from BJH desorption average width (4 V A^{-1})

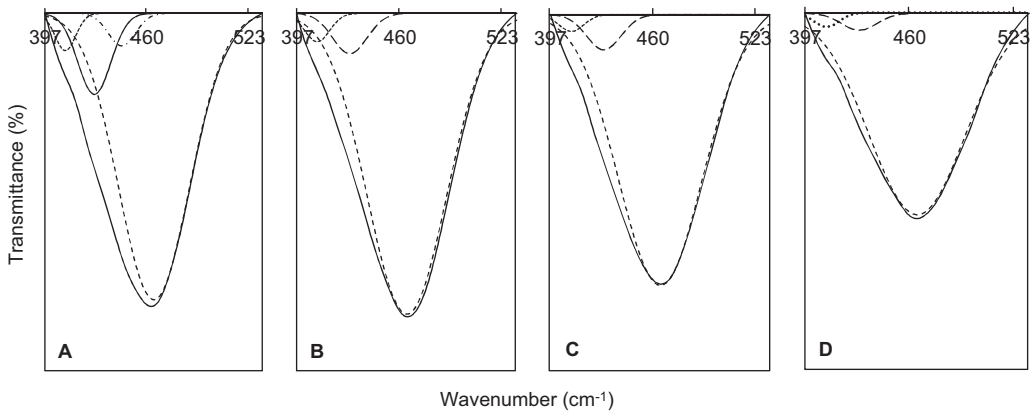

Fig. 7. FTIR spectra of (A) MSN, (B) 1 wt% ZnO/MSN, (C) 5 wt% ZnO/MSN and (D) 10 wt% ZnO/MSN and Gaussian curve-fitting of band at 460 cm^{-1}.

same band confirmed the presence of a broad band at the corresponding range (Fig. 8B), which decreased in intensity by the increasing ZnO content, suggesting a possible insertion of Zn ions into hydroxyl groups of $Si(OH)_4$.

In support of the above conventional FTIR spectroscopy, the MSN and ZnO/MSN samples were also subjected to adsorbed pyridine FTIR in order to study their natural acidic properties; the results are shown in Fig. 9A. The spectra were recorded after adsorption of pyridine at 423 K, followed by removal of pyridine at 573 K. Since the catalysts were outgassed at 573 K, the only acid sites under consideration are strong acid sites that can retain pyridine at the outgassing temperature of 573 K. It was observed that MSN showed almost no band at all in the region of 1600–1400 cm^{-1}, indicating that MSN do not have acidity (Fig. 9Aa). Thus, the silanol groups of MSN that appeared in the 3800–3500 cm^{-1} range were a neutral framework without any Brönsted or Lewis acid sites. However, the introduction of ZnO onto the MSN developed a relatively high band at 1451 cm^{-1} and a small band at 1492 cm^{-1} (Fig. 9Ab–c), which were assigned to a strong Lewis acid site and a weak mixture of Brönsted and Lewis acid sites, respectively [48]. This may be due to the presence of Zn^{2+} cations, which behave as new acidic centers in the MSN.

These results are in line with the conventional FTIR results, which showed interaction between the ZnO species and the silica framework as well as bending Si–OH groups in the MSN. Thus, this result supports the idea that desilication occurred in the MSN framework during preparation of the catalyst, accompanied by Zn ion substitution to form Si–O–Zn bonds. The number of Lewis acid sites increased with increasing ZnO content, and was especially notable in the 10 wt% ZnO/MSN. Similar phenomenon was observed on Zn/HZSM-5 catalyst, in which the introduction of ZnO on HZSM-5 zeolite led to an increased in the number of Lewis acid sites due to the interaction between ZnO and zeolite support [22]. The increase in the number of acidic sites was needed for the activity improvement of the catalyst [49]. Lihitkar et al. and Jiang et al. also reported that the introduction of ZnO onto the mesoporous silica MCM-41 and SBA-15 resulted in the formation of Zn–O–Si bonds [40,50]. In addition, similar observation of a high intensity band at 1450 cm^{-1} in the spectrum of Co/SBA-15 was also reported, indicating the formation of tetrahedrally coordinated Co^{2+} ions with silica support [51].

Carbon monoxide (CO) chemisorption on activated porous materials is widely employed for analysis of active sites on ion-exchanged molecular sieves because of its sensitivity toward electrostatic fields surrounding metal cations [52] and its ability to interact with Brönsted and Lewis acid sites [53]. Fig. 9B shows IR spectra for the adsorption of CO onto MSN and ZnO/MSN catalysts with different ZnO loadings in the 2400–1600 cm^{-1} range. A group of small characteristic bands were observed at 2345, 2159, 2129, and 1645 cm^{-1}. According to data in the literature, the broad band at 2345 cm^{-1} was assigned to adsorbed species of CO_2 that resulted from the oxidation of CO and metal ions [54]. Thus, the appearance of this band in the pure MSN spectrum may possibly

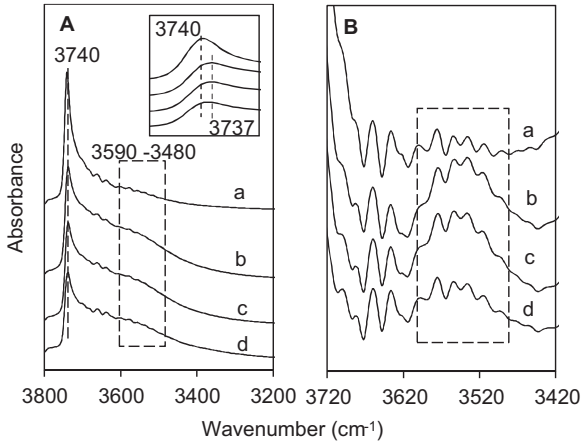

Fig. 8. (A) IR spectra of activated (a) MSN, (b) 1 wt% ZnO/MSN, (c) 5 wt% ZnO/MSN and (d) 10 wt% ZnO/MSN in the region of 3800–3200 cm^{-1} (B) Baseline correction of hydroxyl region at 3720–3420 cm^{-1} (a) MSN, (b) 1 wt% ZnO/MSN, (c) 5 wt% ZnO/MSN and (d) 10 wt% ZnO/MSN.

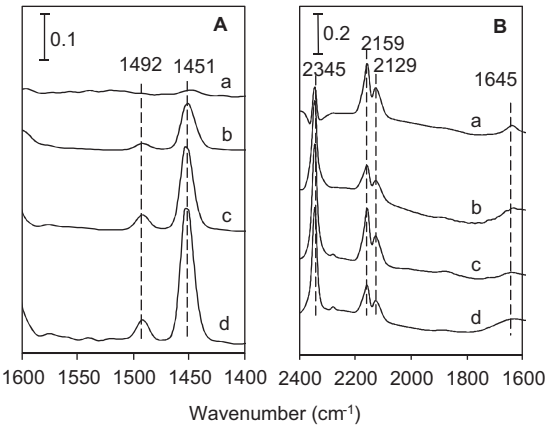

Fig. 9. (A) IR spectra of pyridine adsorbed on activated (a) MSN, (b) 1 wt% ZnO/MSN, (c) 5 wt% ZnO/MSN and (d) 10 wt% ZnO/MSN catalysts at 423 K followed by removal of pyridine at 573 K (B) IR spectra of CO adsorbed on activated (a) MSN, (b) 1 wt% ZnO/MSN, (c) 5 wt% ZnO/MSN and (d) 10 wt% ZnO/MSN catalysts at 123 K.

be due to an interaction between the Si and CO. It was observed that this band became more intense with increasing Zn content, demonstrating the availability of additional Zn^{2+} cations to react with CO. The bands at 2159 and 2129 cm^{-1} corresponded to CO adsorbed on oxidized metal sites that are not in cationic positions, and carbonyl complex species formed with the participation of zinc cation $Zn^{2+}(CO)_2$, respectively, while the small broad band detected at 1645 cm^{-1} is due to carbonate species [55]. This band also became broader with the introduction of Zn, signifying the higher the Zn content, the greater its interaction with CO to form carbonates. The overall reaction mechanism of CO oxidation with Zn metal is as follows,

$$CO + Zn \rightarrow OC \times Zn \quad (2)$$

$$O_2 + Zn \rightarrow 2O \times Zn \quad (3)$$

$$OC \times Zn + O \times Zn \rightarrow {}^{-}OOC \times Zn^{+}\left(CO_3^{2-}\right) + Zn \quad (4)$$

$${}^{-}OOC \times Zn^{+} \overset{\text{rearrangement}}{\rightarrow} CO_2 \times Zn \quad (5)$$

Hence, the above results clearly support the fact that Si–O–Zn groups were undeniably formed in the MSN framework, which is proven by the strong properties of the Lewis acid sites.

3.1.6. Proposed mechanism for formation of ZnO and ZnO/MSN

According to the characterization results and literature, possible reaction pathways for the formation of the ZnO nanorods and ZnO/MSN are shown in Scheme 1A and B, respectively. The electrolysis involved the dissolution of zinc metal at the anode to give zinc cations Zn^{2+} (Scheme 1A) [29],

$$Zn \rightarrow Zn^{2+} + 2e^{-} \quad (6)$$

Then, the presence of hydroxyl groups from water in the solution led to the formation of negatively charged tetrahedron $[Zn(OH)_4]^{2-}$ ions, which interacted electrostatically with the tetrahedral head and a long hydrophobic tail, CTA^{+}, from CTAB to form a reverse micelle system [56]. This $[Zn(OH)_4]^{2-}$ then plays an important role as a building block in the formation of the ZnO structure.

$$Zn^{2+} + 4OH^{-} \rightarrow [Zn(OH)_4]^{2-} \quad (7)$$

The unstable anions may easily be precipitated to form $Zn(OH)_2$, which tends to continuously produce ZnO nuclei [9],

$$[Zn(OH)_4]^{2-} \rightarrow Zn(OH)_2 + 2OH^{-} \quad (8)$$

$$Zn(OH)_2 \rightarrow ZnO + H_2O \quad (9)$$

Due to the strong-acid weak-base properties of the CTAB, it could accelerate the ionization of $[Zn(OH)_4]^{2-}$, as well as react as a capping agent which suppresses the ZnO nuclei to inhibit the lateral growth [57]. Therefore, the ZnO only grows along [001] direction to form the nanorod shape, which is eventually constructed into flower-shaped ZnO (Figs. 2A and 3A).

In parallel, the Zn^{2+} also underwent reduction at the cathode to form zero-valence highly reactive zinc [28], which reacted with H_2O to produce $Zn(OH)_2$ and then went through a similar route as above to produce ZnO.

$$Zn^{2+} + 2e^{-} \rightarrow Zn^{0} \quad (10)$$

$$Zn^{0} + 2H_2O \rightarrow Zn(OH)_2 + H_2 \quad (11)$$

Scheme 1B demonstrates the possible reaction pathways for the formation of ZnO/MSN. The alkaline condition of the system provided an appropriate environment for desilication to occur in the silica network when the MSN was impregnated with the mixture after electrolysis [44]. This prediction was verified by the ^{29}Si NMR result, which showed transformation of the Q^4 site of the pure MSN to Q^3 and Q^2 sites. Subsequently, isomorphous substitution of zinc for silica took place in the silica framework, which simultaneously resulted in the formation of $Si(OH)_4$. This was elucidated by the decrease in intensity of the Si–O–Si peak and possible formation of Si–O–Zn bonds in the FTIR spectra, as well as the detection of a new peak of $Si(OH)_4$ groups in the evacuated FTIR. The adsorbed pyridine and CO FTIR results also supported the formation of Si–O–Zn bonds. However, the nature and structure of the ZnO on the MSN surface are not clear at the present stage and still under investigation.

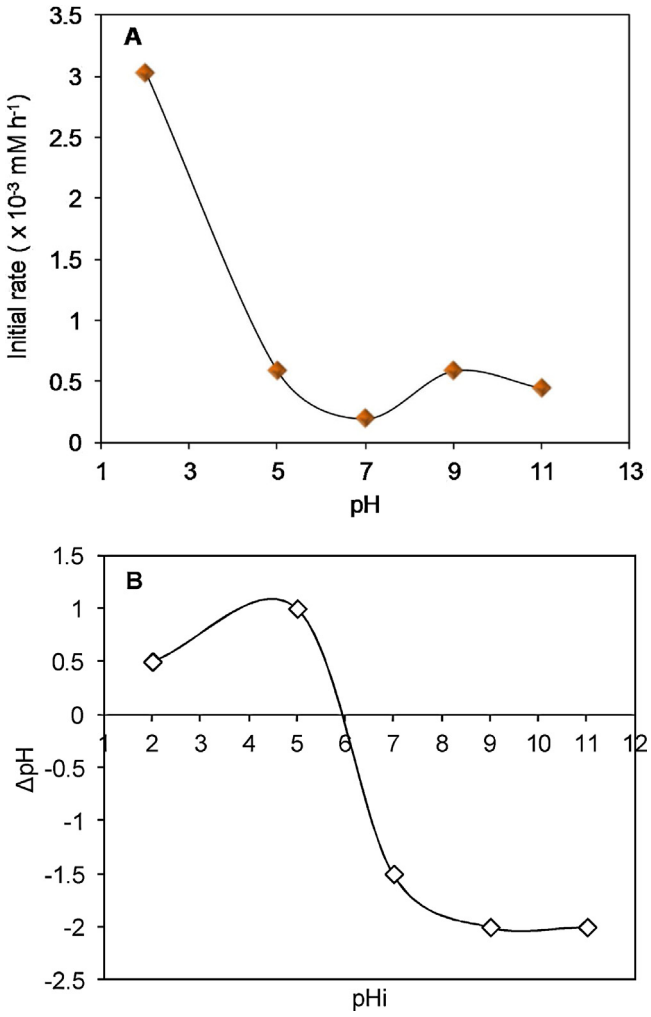

Fig. 10. (A) Effect of pH on decolorization of MO [$C_o = 3.06 \times 10^{-2}$ mM; $W = 1$ g L^{-1}; $t = 8$ h; 5 wt% ZnO/MSN; 303 K] and (B) The isoelectric point (pH_{pzc}) of 5 wt% ZnO/MSN catalyst.

3.2. Photocatalytic testing

3.2.1. Effect of pH

The pH plays a significant role in the photodecolorization of dyes because of all the interactions between the catalyst surface and dye molecules; the formation of charge depends on the pH of the solution system [19]. Therefore, a suitable pH needs to be found in order to obtain the optimum photocatalytic activity. Herein, the effect of pH was studied in the range of 2–11 in the presence of the 5 wt% ZnO/MSN catalyst; the results are shown in Fig. 10A. It can be seen that the greatest decolorization was achieved at pH 2, while further increases in pH resulted in a lower efficiency of

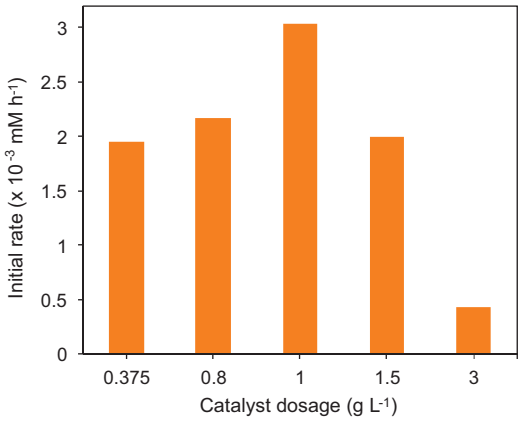

Fig. 11. Effect of catalyst dosage on decolorization of MO [$C_o = 3.06 \times 10^{-2}$ mM; pH = 2; t = 8 h; 5 wt% ZnO/MSN; 303 K].

reaction. The performance of the catalyst is expected be affected by the electrostatic interaction between the positively charged catalyst surfaces with the negatively charged MO. The abundance of H^+ ions at pH 2 might provide an appropriate surrounding for the dye molecules to be attracted toward the ZnO/MSN sites, facilitating the formation of more hydroxyl radicals from the ZnO and hence resulting in higher photocatalytic activity. In contrast, increasing the pH led to an increase in the number of hydroxyl groups, causing a competition with the MO ions in the system and thus reducing the photocatalytic performance.

The effect of pH could also be explained by the amphoteric behavior of the semiconductor when the photoreaction occurs on its surface [37]. This behavior can be described on the basis of the point zero charge (pH_{pzc}) of the ZnO/MSN, which was determined to be pH 6 (Fig. 10B). At pH values less than pH_{pzc}, the surface of the ZnO/MSN became positively charged and electrostatically attracted the negatively charged MO anions. Therefore, the photoreaction performed well in acidic rather than in basic conditions. A similar phenomenon was also observed in the decolorization of MO in the presence of TiO_2/ZnS/chitosan catalyst [58].

3.2.2. Effect of catalyst dosage

Fig. 11 demonstrates the effect of catalyst dosage on the initial rate of MO decolorization, which was studied at pH 2 using a 3.06×10^{-2} mM MO solution. It was observed that the decolorization rate was increased by increasing the dose of catalyst from 0.375 to 1 g L^{-1}. The most rapid decolorization was achieved when 1 g L^{-1} of 5 wt% ZnO/MSN was used, but a further increase in catalyst dosage resulted in a decrease in the reaction rate. The higher the catalyst dosage, the greater the number of MO moieties adsorbed onto the active sites of the catalyst surface, thus leading to an increase in the number of photons being absorbed, resulting in more rapid decolorization [59]. However, excess catalyst produced greater turbidity in the system, which scattered the light, reducing its penetration and ability to reach the active sites, thus inhibiting photodecolorization [18]. Similar results have been observed in the literature on decolorization of MO or textile dye wastewater using ZnO based photocatalysts, respectively [60].

3.2.3. Effect of ZnO loading

The effect of ZnO loading onto the MSN was examined in the range of 1–10 wt% toward an initial rate of MO decolorization (Fig. 12A). The values represented the initial decolorization rate of MO per unit surface area of the catalyst given by BET data. The 5 wt% ZnO/MSN gave the highest value of 6.2×10^{-3} h^{-1} m^{-2} g^{-1}, while both 1 wt% ZnO/MSN and 10 wt% ZnO/MSN gave values reduced by one-third. The efficiency of the decolorization could be influenced by the metal dispersion on the support surface, the structure of the catalyst, the band gap of the catalyst or a synergetic effect between the metal and support. The 5 wt% ZnO/MSN shows highest value compared to 1 wt% ZnO/MSN and 10 wt% ZnO/MSN, suggesting good dispersion of ZnO on the MSN surface, which led to a faster rate of reaction. In contrast, ZnO might be agglomerated on the surface of 10 wt% ZnO/MSN, which then reduced the surface area available for MO attraction and light penetration for an efficient photocatalytic reaction [61].

For a detailed study of their optical properties and crystal defects, the catalysts were subjected to photoluminescence (PL); the spectra are shown in Fig. 12B. All the samples were measured at an excitation wavelength of 325 nm. As shown in the inset figure, the PL spectrum of bare prepared ZnO consisted of two distinct sharp and broad emission bands at 386 nm in the UV region and 514 nm in the visible region. The UV emission was generated by the free-excitation recombination, while the green emission (deep level emission) appeared because of impurities and structural defects in the deposited structures. The UV emission signified the recombination of a photogenerated hole with an electron occupying the oxygen vacancies, while the green emission signified the recombination of electrons in single occupied oxygen vacancies in ZnO [62]. Generally, highly crystalline ZnO shows a dominant UV emission with a weak green emission. Thus, it could be concluded that the ZnO electrosynthesized in this study is relatively high in crystallinity.

It was observed that the peak intensity of ZnO/MSN was increased by increasing the ZnO content, with 10 wt% ZnO/MSN demonstrating the highest intensity. This may be because the addition of a certain amount of ZnO increased the content of surface

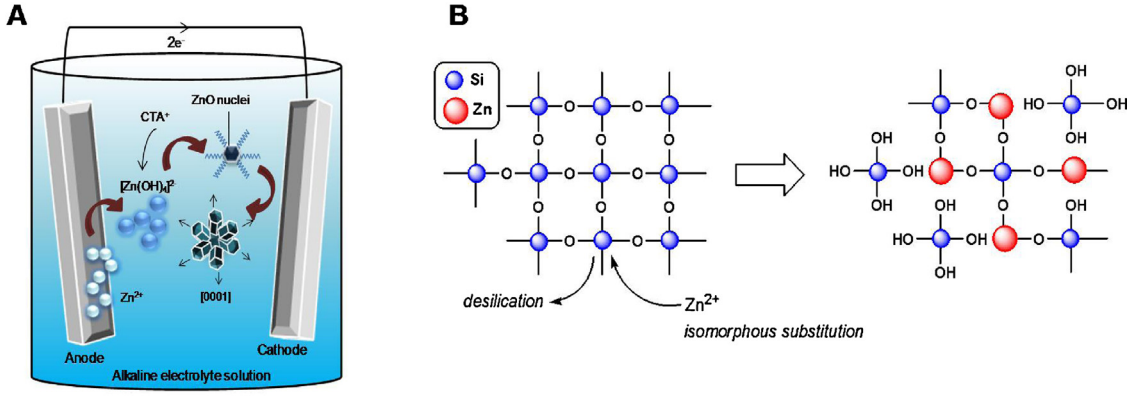

Scheme 1. Possible reaction pathways for formation of (A) ZnO and (B) ZnO/MSN catalysts.

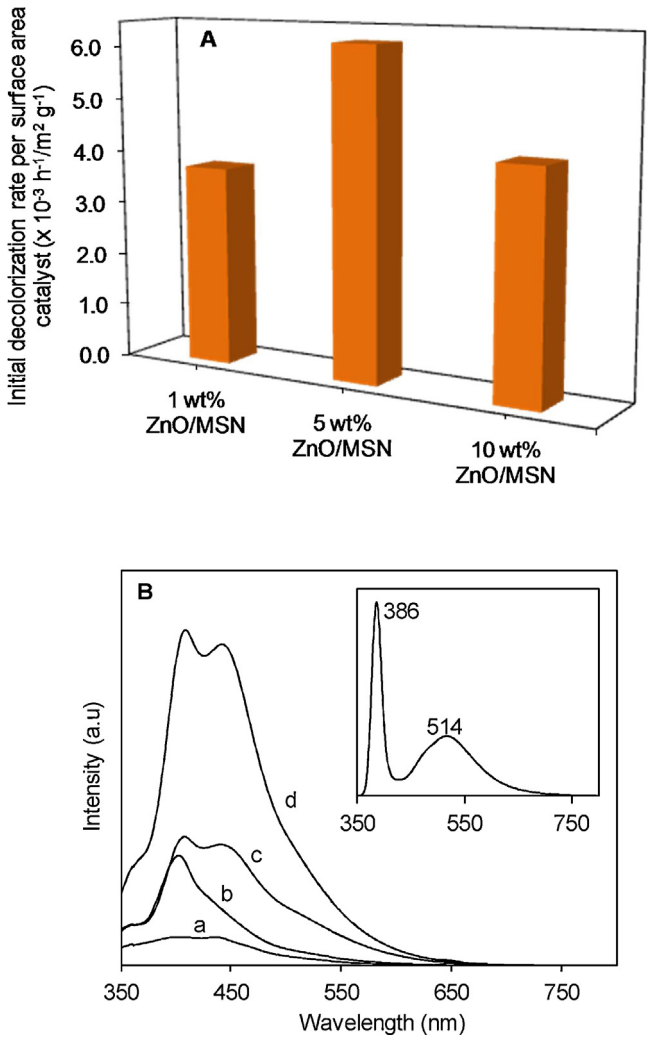

Fig. 12. (A) Effect of ZnO loading on decolorization of MO [$C_o = 3.06 \times 10^{-2}$ mM; pH = 2; $t = 8$ h; $W = 1$ g L^{-1}; 303 K] and (B) PL spectra of the catalysts with the excitation wavelength of 325 nm (a) MSN, (b) 1 wt% ZnO/MSN, (c) 5 wt% ZnO/MSN and (d) 10 wt% ZnO/MSN catalysts. Inset figure shows PL spectra for ZnO.

oxygen vacancies and defects, which affected the intensity and response range of the PL signals [63]. On the other hand, the peak positions in the PL spectra for an ascending ZnO content apparently shifted to longer wavelengths, implying a decrease in the band gap energy of the ZnO [62]. However, it was reported that the higher the PL intensity, the higher the recombination rate of the photoinduced electron–hole pair, which resulted in lower photocatalytic activity of the catalyst [62]. This fact may explain the higher decolorization rate shown by the 5 wt% ZnO/MSN catalyst as compared to 10 wt% ZnO/MSN. In contrast, the 1 wt% ZnO/MSN catalyst showed a slightly different pattern of PL emission compared to the others, with a trace emission at 462 nm, signifying fewer oxygen anion vacancies created at its interface [64]. The lack of oxygen vacancies and defects on the surface of the catalyst caused a deficiency in photoinduced electron captures, which led to recombination of photoinduced electron–hole pairs, thus decreasing the efficiency of the decolorization [64]. In addition, the absence of oxygen vacancies could also inhibit the adsorption of O_2, which also plays an important role in promoting the oxidation of organic dye pollutants. These factors may explain why 1 wt % ZnO was insufficient for efficient decolorization.

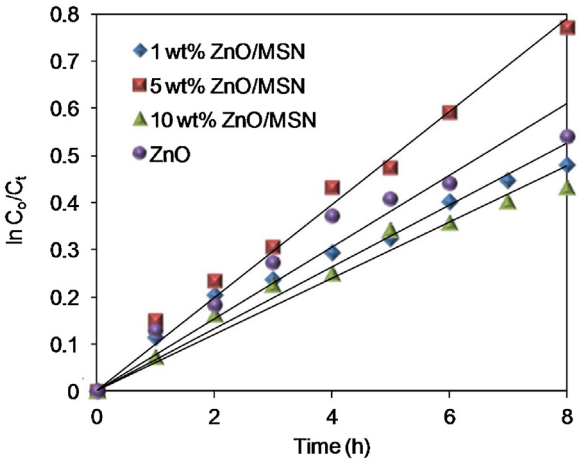

Fig. 13. Photodecolorization kinetics of MO using different catalysts.

3.3. Kinetic analysis

Generally, the kinetics of most organic compounds that undergo photocatalytic reactions are described by a pseudo first-order model, which is rationalized in terms of the Langmuir–Hinshelwood model modified to accommodate reactions occurring at a solid–liquid interface [18,62]. In this study, a series of reactions over bare ZnO and ZnO/MSN with different metal loadings ranging from 1–10 wt% were carried out under UV irradiation in order to study the kinetics of MO decolorization; the results are shown in Fig. 13. The linearity of the plot of $\ln(C_o/C_t)$ vs. irradiation time verified that the reaction process approximately followed the pseudo-first order kinetics model, which is expressed by the simplified equation as follows [65],

$$\ln\left(\frac{C_o}{C_t}\right) = kt \quad (12)$$

where k is the pseudo first-order rate constant and C_0 and C_t are the concentrations of MO at initial time and time t, respectively. The data were fitted to the corresponding logarithmic expression to obtain an apparent rate constant, k. Table 2 lists the values of k when using bare ZnO and ZnO/MSNs. The value of k' over the surface area of the each catalyst was also given for comparison. It is clearly observed that 5 wt% ZnO/MSN gave greater k values than the others, indicating its efficiency at decolorization. These results also illustrate the important role of MSN as a support in reducing the amount of Zn used, which is beneficial from an economic point of view. The formation of Si–O–Zn bonds in the silica framework of MSN may act as active sites that produce a higher reaction rate of ZnO/MSNs compared to bare ZnO.

3.4. Evaluation of zinc leaching and catalyst stability

To study the zinc leaching into the solution, the sample was kept in dark for 1 h and then irradiated under UV light for several hours (2, 4, 6 and 8 h) using an amount of 1 g L^{-1} 5 wt%

Table 2
The kinetics parameters of photodecolorization using different catalysts.

Catalyst	$k^a \times 10^{-2}$ (h^{-1})	$k^b \times 10^{-4}$ (h^{-1})
ZnO	7.64	18.2
1 wt% ZnO/MSN	5.96	1.23
5 wt% ZnO/MSN	9.93	2.30
10 wt% ZnO/MSN	2.53	0.73

[a] Apparent rate constant.
[b] The k values were normalized with the surface area.

Table 3
Zn leaching in the solution determined by MP-AES. Figures and scheme captions.

Condition		Zn detected in the solution	
		$mM \times 10^{-2}$	%
In dark		1.98	2.60
Irradiation (h)	2	2.00	2.62
	4	2.12	2.77
	6	2.26	2.95
	8	2.27	2.97

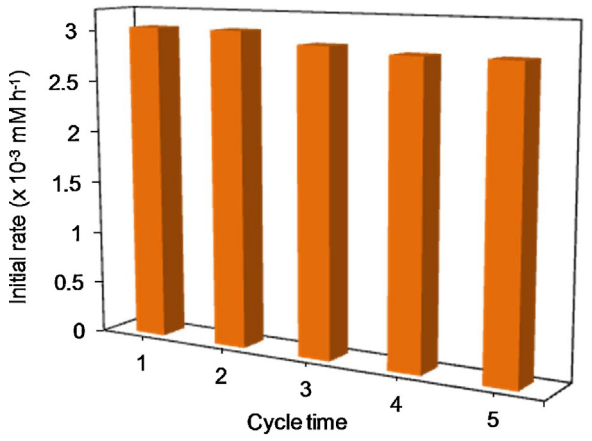

Fig. 14. Stability of 5 wt% ZnO/MSN on decolorization of MO [$C_o = 3.06 \times 10^{-2}$ mM; pH = 2; t = 8 h; 303 K].

ZnO/MSN in 3.06×10^{-2} mM MO solution at pH 2. The samples then were subjected to microwave plasma-atomic emission spectrometer (MP-AES). The amount of zinc detected in the solution was less that 2.30×10^{-2} mM (<3.0%) as listed in Table 3. Only a small amount of zinc was leached, indicating the zinc present on the catalyst surface which can be related to Zn–O–Si bond plays an important role in the photocatalytic reaction. Similar result were also reported in the literature, in which the maximum decolorization of reactive black 5 dye (~100%) and trypan blue dye (89.2%) were achieved at acidic pH (pH 4 and 5) when using ZnO and Se doped ZnO nanoparticles, respectively [66,67].

The stability of the catalyst was evaluated by recycling experiments and the result is presented in Fig. 14. For each new cycle, the catalyst was reused for the decolorization of a fresh MO solution. The initial concentration of MO was remained constant (3.06×10^{-2} mM) at pH 2 for 8 h irradiation time. Then, the catalyst was recycled after centrifuged, washed and calcined at 823 K for 3 h for every cycle. As shown in the figure, after five cycle, 5 wt% ZnO/MSN catalyst was still active with just a small decrease in the decolorization rate. The decrease in photocatalytic efficiency was probably due to the decrease in surface area of the catalyst which resulted from the catalyst aggregation after several cycles by the heat treatment (calcination) [68].

4. Conclusion

In this study, ZnO/MSN catalysts were prepared via sequence electrosynthesis and impregnation methods. The physicochemical properties of the synthesized catalysts were studied by XRD, ^{29}Si NMR, FE-SEM, TEM, FTIR, and PL. The XRD result showed that the introduction of zinc species onto the MSN shifted the (1 0 0) reflection peak to slightly higher angles, suggesting the presence of ZnO on the internal pore walls of the support. From the ^{29}Si NMR results, the $(\equiv SiO)_4Si$ peak of the parent MSN was observed to transform to two new shoulder peaks corresponding to $(\equiv SiO)_2Si$ and $(\equiv SiO)_3Si$ when ZnO was introduced into the MSN, proving desilication was occurring in the MSN framework. The FTIR data suggested that isomorphous substitution was taking place after the desilication due to the decrease in intensity and shift of the Si–O–Si peaks and the detection of possible Zn–O–Si bonds. The increase in the number of Lewis acid sites with increasing ZnO content when the samples were subjected to adsorbed pyridine FTIR also supported the formation of Si–O–Zn bonds. The FTIR of adsorbed CO confirmed that the increase in Zn loading resulted in more Zn^{2+} cations reacting with CO. According to the PL analysis, it was verified that 5 wt% ZnO/MSN was the most effective photocatalyst for decolorization of MO. The kinetic study showed that the decolorization process followed pseudo first-order kinetics with a reaction rate of 9.93×10^{-2} h^{-1}. In addition, the stability test revealed that the catalyst was still stable after five cycling runs with a small Zn leached detected in the solution.

Acknowledgment

The authors are grateful for the financial support by the Research University Grant from Universiti Teknologi Malaysia (Grant No. 01H59), the Exploration Research Grant Scheme and the awards of MyPhD Scholarship (Nurfatehah Wahyuny Che Jusoh) from Ministry of Higher Education, and to the Hitachi Scholarship Foundation for their support.

References

[1] A.A. Jalil, S. Triwahyono, S.H. Adam, N.D. Rahim, M.A.A. Aziz, N.H.H. Hairom, N.A.M. Razali, M.A.Z. Abidin, M.K.A. Mohamadiah, J. Hazard. Mater. 181 (2010) 755–762.
[2] M.A. Rauf, S. Salman Ashraf, Chem. Eng. J. 209 (2012) 520–530.
[3] R.A. Damodar, S.-J. You, S.-H. Ou, Sep. Purif. Technol. 76 (2010) 64–71.
[4] S.H. Adam, A.A. Jalil, S. Triwahyono, Desalin. Water Treat. 49 (2012) 337–347.
[5] F. Harrelkas, A. Azizi, A. Yaacoubi, A. Benhammou, M.N. Pons, Desalination 235 (2009) 330–339.
[6] J. Zhai, X. Tao, Y. Pu, X.-F. Zeng, J.-F. Chen, Appl. Surf. Sci. 257 (2010) 393–397.
[7] J.S. Wu, C.H. Liu, K.H. Chu, S.Y. Suen, J. Membr. Sci. 309 (2008) 239–245.
[8] J.H. Sun, S.Y. Dong, Y.K. Wang, S.P. Sun, J. Hazard. Mater. 172 (2009) 1520–1526.
[9] R. Wahab, I.H. Hwang, Y.-S. Kim, H.-S. Shin, Chem. Eng. J. 168 (2011) 359–366.
[10] R. Saravanan, V.K. Gupta, V. Narayanan, A. Stephen, J. Mol. Liq. 181 (2013) 133–141.
[11] S. Anandan, A. Vinu, N. Venkatachalam, B. Arabindoo, V. Murugesan, J. Mol. Catal. A: Chem. 256 (2006) 312–320.
[12] C. Bouvy, W. Marine, B.-L. Su, Chem. Phys. Lett. 438 (2007) 67–71.
[13] L.I. Burova, D.I. Petukhov, A.A. Eliseev, A.V. Lukashin, Y.D. Tretyakov, Superlattices Microstruct. 39 (2006) 257–266.
[14] C. Cannas, M. Mainas, A. Musinu, G. Piccaluga, Compos. Sci. Technol. 63 (2003) 1187–1191.
[15] C. Bouvy, F. Piret, W. Marine, B.L. Su, Chem. Phys. Lett. 433 (2007) 350–354.
[16] M. Silva, M.J.F. Calvete, N.P.F. Gonçalves, H.D. Burrows, M. Sarakha, A. Fernandes, M.F. Ribeiro, M.E. Azenha, M.M. Pereira, J. Hazard. Mater. 233–234 (2012) 79–88.
[17] H. Sun, X. Feng, S. Wang, H.M. Ang, M.O. Tadé, Chem. Eng. J. 170 (2011) 270–277.
[18] N. Sapawe, A.A. Jalil, S. Triwahyono, S.H. Adam, N.F. Jaafar, M.A.H. Satar, Appl. Catal., B: Environ. 125 (2012) 311–323.
[19] N.F. Jaafar, A. Abdul Jalil, S. Triwahyono, M.N. Muhd Muhid, N. Sapawe, M.A.H. Satar, H. Asaari, Chem. Eng. J. 191 (2012) 112–122.
[20] A.A. Jalil, M.A.H. Satar, S. Triwahyono, H.D. Setiabudi, N.H.N. Kamarudin, N.F. Jaafar, N. Sapawe, R. Ahamad, J. Electroanal. Chem. 701 (2013) 50–58.
[21] N. Sapawe, A.A. Jalil, S. Triwahyono, Chem. Eng. J. 225 (2013) 254–265.
[22] S. Triwahyono, A.A. Jalil, R.R. Mukti, M. Musthofa, N.A.M. Razali, M.A.A. Aziz, Appl. Catal., A: Gen. 407 (2011) 91–99.
[23] S. Triwahyono, A.A. Jalil, M. Musthofa, Appl. Catal., A: Gen. 372 (2010) 90–93.
[24] H.D. Setiabudi, A.A. Jalil, S. Triwahyono, N.H.N. Kamarudin, R.R. Mukti, Appl. Catal., A: Gen. 417–418 (2012) 190–199.
[25] M. Selvaraj, A. Pandurangan, K.S. Seshadri, P.K. Sinha, K.B. Lal, Appl. Catal., A: Gen. 242 (2003) 347–364.
[26] A.H. Karim, A.A. Jalil, S. Triwahyono, S.M. Sidik, N.H.N. Kamarudin, R. Jusoh, N.W.C. Jusoh, B.H. Hameed, J. Colloid Interface Sci. 386 (2012) 307–314.
[27] A.A. Jalil, N. Fatimah, A. Panjang, S. Akhbar, M. Sundang, N. Tajuddin, S. Triwahyono, J. Hazard. Mater. 148 (2007) 1–5.
[28] A.A. Jalil, N. Kurono, M. Tokuda, Tetrahedron 58 (2002) 7477–7484.
[29] A.A. Jalil, N. Kurono, M. Tokuda, Synlett (2001) 1944–1946.
[30] S. Mustafa, B. Dilara, K. Nargis, A. Naeem, P. Shahida, Colloids Surf., A 205 (2002) 273–282.
[31] U. Hiroyuki, Mater. Lett. 63 (2009) 1489–1492.
[32] P. Ma, Y. Wu, Z. Fu, W. Wang, J. Alloys Compd. 509 (2011) 3576–3581.

[33] S. Singh, K.C. Barick, D. Bahadur, CrystEngComm (2013) 4631–4639.
[34] L.J. Chen, Y.J. Chuang, Mater. Lett. 68 (2012) 460–462.
[35] D. Zhao, C. Nie, Y. Zhou, S. Xia, L. Huang, Q. Li, Catal. Today 68 (2001) 11–20.
[36] G.D. Mihai, V. Meynen, M. Mertens, N. Bilba, P. Cool, E.F. Vansant, J. Mater. Sci. 45 (2010) 5786–5794.
[37] K. Hayat, M.A. Gondal, M.M. Khaled, S. Ahmed, A.M. Shemsi, Appl. Catal., A: Gen. 393 (2011) 122–129.
[38] Q.R. Hu, S.L. Wang, W.H. Tang, Mater. Lett. 64 (2010) 1822–1824.
[39] S. Panigrahi, D. Basak, Chem. Phys. Lett. 511 (2011) 91–96.
[40] P.B. Lihitkar, S. Violet, M. Shirolkar, J. Singh, O.N. Srivastava, R.H. Naik, S.K. Kulkarni, Mater. Chem. Phys. 133 (2012) 850–856.
[41] W. Zeng, Z. Wang, X.-F. Qian, J. Yin, Z.-K. Zhu, Mater. Res. Bull. 41 (2006) 1155–1159.
[42] G. Du, S. Lim, Y. Yang, C. Wang, L. Pfefferle, G.L. Haller, Appl. Catal., A: Gen. 302 (2006) 48–61.
[43] J. Klinowski, Colloids Surf. 36 (1989) 133–154.
[44] S. Abelló, A. Bonilla, J. Pérez-Ramírez, Appl. Catal., A: Gen. 364 (2009) 191–198.
[45] Y. Xiong, L.Z. Zhang, G.-Q. Tang, G.-L. Zhang, W.-J. Chen, J. Lumin. 110 (2004) 17–22.
[46] W.-H. Zhang, J.-L. Shi, L.-Z. Wang, D.-S. Yan, Chem. Mater. 12 (2000) 1408–1413.
[47] B. Gil, Ł. Mokrzycki, B. Sulikowski, Z. Olejniczak, S. Walas, Catal. Today 152 (2010) 24–32.
[48] S. Triwahyono, T. Yamada, H. Hattori, Appl. Catal., A: Gen. 242 (2003) 101–109.
[49] S.S. Kum, B.Y. Jo, S.H. Moon, Appl. Catal., A: Gen. 365 (2009) 79–87.
[50] Q. Jiang, Z.Y. Wu, Y.M. Wang, Y. Cao, C.F. Zhou, J.H. Zhu, J. Mater. Chem. 16 (2006) 1536–1542.
[51] Á. Szegedi, M. Popova, C. Minchev, J. Mater. Sci. 44 (2009) 6710–6716.
[52] W.J. Kim, I.Y. Ahn, J.H. Lee, S.H. Moon, Catal. Commun. 24 (2012) 52–55.
[53] K. Góra-Marek, M. Derewiński, P. Sarv, J. Datka, Catal. Today 101 (2005) 131–138.
[54] Z.M. El-Bahy, A.I. Hanafy, M.M. Ibrahim, M. Anpo, J. Mol. Catal. A: Chem. 344 (2011) 111–121.
[55] M. Ahrens, O. Marie, P. Bazin, M. Daturi, J. Catal. 271 (2010) 1–11.
[56] D. Geetha, T. Thilagavathi, Dig. J. Nanomater. Biostruct. 5 (2010) 297–301.
[57] U.N. Maiti, S. Nandy, S. Karan, B. Mallik, K.K. Chattopadhyay, Appl. Surf. Sci. 254 (2008) 7266–7271.
[58] H. Zhu, R. Jiang, Y. Fu, Y. Guan, J. Yao, L. Xiao, G. Zeng, Desalination 286 (2012) 41–48.
[59] N. Dubey, S.S. Rayalu, N.K. Labhsetwar, R.R. Naidu, R.V. Chatti, S. Devotta, Appl. Catal., A: Gen. 303 (2006) 152–157.
[60] H.Y. Zhu, L. Xiao, R. Jiang, G.M. Zeng, L. Liu, Chem. Eng. J. 172 (2011) 746–753.
[61] H. Wang, S. Baek, J. Lee, S. Lim, Chem. Eng. J. 146 (2009) 355–361.
[62] N. Sapawe, A.A. Jalil, S. Triwahyono, R.N.R.A. Sah, N.W.C. Jusoh, N.H.H. Hairom, J. Efendi, Appl. Catal., A: Gen. 456 (2013) 144–158.
[63] J. Liqiang, Q. Yichun, W. Baiqi, L. Shudan, J. Baojiang, Y. Libin, F. Wei, F. Honggang, S. Jiazhong, Sol. Energy Mater. Sol. Cells 90 (2006) 1773–1787.
[64] Q. Jiang, Z.Y. Wu, Y.M. Wang, Y. Cao, C.F. Zhou, J.H. Zhu, J. Mater. Chem. 16 (2006) 1536–1542.
[65] Y.J. Do, J.H. Kim, J.H. Park, S.S. Park, S.S. Hong, C.S. Suh, G.D. Lee, Catal. Today 101 (2005) 299–305.
[66] S. Kansal, N. Kaur, S. Singh, Nanoscale Res. Lett. 4 (2009) 709–716.
[67] B.P. Nenavathu, A.V.R. Krishna Rao, A. Goyal, A. Kapoor, R.K. Dutta, Appl. Catal., A: Gen. 459 (2013) 106–113.
[68] M. Huang, C. Xu, Z. Wu, Y. Huang, J. Lin, J. Wu, Dyes Pigm. 77 (2008) 327–334.